



## Gross theory of $\beta$ decay by considering the spin-orbit splitting from relativistic Hartree-Bogoliubov theory

J. Y. Fang (方基宇) , J. Chen (陈静), and Z. M. Niu (牛中明) \*

*School of Physics and Optoelectronic Engineering, Anhui University, Hefei 230601, China*



(Received 2 May 2021; revised 7 June 2022; accepted 1 November 2022; published 16 November 2022)

Nuclear  $\beta$ -decay half-lives are predicted with the so-called gross theory, which is improved by including the spin-orbit splitting from relativistic Hartree-Bogoliubov theory. The calculated differences between the Gamow-Teller and Fermi transition energies are in excellent agreement with experimental data for Zr, Sn, and Pb isotopes. The influences of the  $Q$  value and the integrated Fermi function on the calculations of  $\beta$ -decay half-lives are carefully studied. Based on the mass predictions of the latest Weizsäcker-Skyrme model, the half-lives from Ca to Pb isotopes are systematically calculated. It is found that the Weizsäcker-Skyrme model well reproduces the experimental data with accuracy better than that of quasiparticle random-phase approximation approaches. When extrapolated to the unknown region, our results are generally close to those from the Skyrme finite-amplitude method. This improved gross theory can be employed to calculate half-lives based on mass predictions of various models and hence can provide relatively consistent half-life inputs for the  $r$ -process studies.

DOI: [10.1103/PhysRevC.106.054318](https://doi.org/10.1103/PhysRevC.106.054318)

### I. INTRODUCTION

Nuclear  $\beta$  decay is a fundamental and important decay mode. There are more than 3000 known nuclei, of which more than 2000 mainly undergo  $\beta$  decay [1]. It contains a wealth of information on nuclear structure, such as nuclear masses [2], shapes [3], energy levels [4], and shell gaps [5]. Moreover, nuclear  $\beta$ -decay also plays an important role in nuclear astrophysics [6,7]. It governs the matter flow between neighboring isotopic chains of the rapid neutron-capture process ( $r$ -process) and roughly sets the  $r$ -process timescale, so it is a key process for the production of heavy elements in the Universe [8,9].

During the past decades, much progress has been made in the measurement of  $\beta$ -decay half-lives. The measurements have been extended to the region far from the stability line now, such as the region beyond the  $N = 82$  shell gap [10,11], the region important to the formation of the rare-earth peak of the  $r$ -process [12], and the region approaching the  $r$ -process path near  $N = 126$  [13]. However, the half-lives of many nuclei on the  $r$ -process path still cannot be measured, especially for the nuclei with  $N = 126$ . Therefore, theoretical predictions of nuclear half-lives are essential to the  $r$ -process studies. There are mainly four kinds of theories predicting nuclear  $\beta$ -decay half-lives: the empirical formula [14,15], the gross theory [16–19], the proton-neutron quasiparticle random-phase approximation (QRPA) [20–23], and the shell model [24–27]. The empirical formula is simple to calculate nuclear  $\beta$ -decay half-lives with high accuracy, while it neglects the microscopic information of  $\beta$ -decay transitions, which may affect its extrapolation ability. The QRPA ap-

proaches based on the covariant density-functional theory [28–31] and the finite-range droplet model (FRDM) [32] have been widely employed to calculate  $\beta$ -decay half-lives, which can be applied to most nuclei in the nuclear chart except for a few very light nuclei. However, conventional QRPA calculations in the matrix form are very time-consuming, so the finite-amplitude method (FAM) was developed to solve QRPA equations [33,34], which has been used to systematically predict half-lives of medium-mass and heavy neutron-rich isotopes recently [35,36]. The nuclear shell model includes the detailed structure of the  $\beta$ -strength function and can be successfully applied to describe  $\beta$ -decay half-lives of light nuclei or nuclei near magic numbers. However, the dimension of configuration space of the shell model increases rapidly with the increase of the number of valence nucleons, so it is impossible to make systematic half-life calculations for all neutron-rich nuclei.

Based on a summation rule for the  $\beta$ -decay strength function, the gross theory treats the transitions to all final nuclear levels in a statistical way. The strength function in the gross theory corresponds to the intensity of  $\beta$ -decay to each excited level of daughter nuclei. The location of its peak is roughly determined by the sum rule of the intensities, and the volume of the broaden foot region is restricted by the energy-weighted sum rules of intensities. For  $\beta^-$  decay, its foot part is dominant, while the peak part could play dominant contributions for  $\beta^+$  decay. The gross theory was proposed in Ref. [16], in which nuclear  $\beta$ -decay half-lives can be easily predicted only with the input of  $\beta$ -decay energies. It was later improved by including a revised treatment of the even-odd mass difference [37] and the first-forbidden transitions [38]. The gross theory was further improved by employing the single-particle strength function having a peak with a long tail, which is usually named GT2 [17]. By taking into account the

\* zmnium@ahu.edu.cn

shell effects of the parent nuclei, the semi-gross theory was developed [18], whose overall accuracy is comparable with the overall accuracies of the microscopic models. The change in parity at the single-particle level was considered in the gross theory, which systematically reduces the discrepancies of theoretical predictions from experimental half-lives for nuclei near the magic numbers [19]. Compared with the microscopic models, the gross theory can predict half-lives of nuclei on the whole nuclear chart with less computational cost, while its accuracy is still comparable with the accuracies of the microscopic models. Recently, the change of spin and parity between neutron and proton single-particle levels has been included to improve the predictive power of the gross theory [39]. In addition, the influence of the axial-vector coupling constant, the energy distribution function, and the antineutrino mass on the  $\beta$ -decay half-lives is also investigated within the gross theory of  $\beta$  decay [40,41].

The  $r$ -process studies necessitate many nuclear physics inputs, among which nuclear masses,  $\beta$ -decay properties, and neutron-capture rates are essential to make dynamic  $r$ -process simulations. Recently, nuclear mass predictions have achieved great progress with both microscopic and macroscopic-microscopic mass models. For the microscopic models, the nonrelativistic Hartree-Fock-Bogoliubov mass models with Skyrme force [42] (SHFB) or Gogny force [43] have been developed with an accuracy of about 600 keV. The accuracies of relativistic mean-field mass models have also been improved from about 2.5 MeV [44] to about 1.5 MeV [45,46]. For the macroscopic-microscopic models, the latest versions of the FRDM [47] have been developed together with the self-consistent calculations of  $\beta$ -decay properties. The accuracy of the Weizsäcker-Skyrme (WS) model has been improved to about 300 keV [48], which is the best value for the accuracies of present macroscopic-microscopic mass models. Based on a spherical basis with an improved even-odd term, another famous macroscopic-microscopic model—the Koura-Tachibana-Uno-Yamada (KTUY) [49] mass model—was developed with an accuracy of about 700 keV. Furthermore, various approaches have been proposed to improve the accuracies of these nuclear mass models, e.g., the image reconstruction technique [50], the radial basis function approach [51,52], and the machine-learning technique [53–55]. However, the self-consistent  $\beta$ -decay calculations based on these high-accuracy mass predictions are scarce.

The gross theory provides an effective tool to make  $\beta$ -decay calculations with the decay energies from the reliable mass models. The  $Q$  value is a key physical quantity for the study of  $\beta$ -decay half-lives, which is the only input of the gross theory. Taking the KTUY and WS4 mass models as examples, the influence of the  $Q$  value on the calculation of  $\beta$ -decay half-lives is studied with an improved integrated Fermi function. Apart from the  $\beta$ -decay energies, the properties of the Gamow-Teller transition are also very important in the predictions of  $\beta$ -decay half-lives, which will be carefully constructed to reproduce the experimental values in this work. It is well known that the relativistic density functional theory naturally includes the nucleon spin degree of freedom [56,57] and gives reasonable spin-orbit potential without any extra model parameters. Therefore, we employ the relativistic

Hartree-Bogoliubov (RHB) theory [58–60] to extract the nuclear average spin-orbit splitting, which is crucial to reliably describe the Gamow-Teller transition central energies.

The paper is organized as follows. A brief introduction of the gross theory is presented in Sec. II, and special attention is focused on the improvement of the gross theory with the average spin-orbit splitting from the RHB theory. Based on the  $\beta$ -decay energies from the latest version of the WS model (WS4) [48], nuclear  $\beta$ -decay half-lives are calculated, and the corresponding results and discussion are given in Sec. III. Finally, a summary is presented in Sec. IV.

## II. THEORETICAL FRAMEWORK

### A. Gross theory of $\beta$ decay

Proceeding from the Fermi theory of  $\beta$  decay, the total  $\beta$ -decay rate of allowed and superallowed transitions in the approximation is written as

$$\lambda = \frac{m_e^5 c^4}{2\pi^3 \hbar^7} \sum_E \sum_{\Omega=F,GT} G_{\Omega}^2 |M_{\Omega}(E)|^2 f(-E), \quad (1)$$

where  $m_e$  is the electron mass;  $G_F$  and  $G_{GT}$  are the coupling constants of the Fermi and Gamow-Teller interactions, respectively;  $E$  is the energy difference between the initial state and the final state; and  $f(-E)$  is the integrated Fermi function. In the gross theory [16], it is assumed that the final level density is large enough to replace the summation over transition states by an integration as

$$\lambda \approx \frac{m_e^5 c^4}{2\pi^3 \hbar^7} \int_{-Q}^0 \sum_{\Omega=F,GT} G_{\Omega}^2 |M_{\Omega}(E)|^2 f(Z, E_m) dE, \quad (2)$$

with  $E_m = m_e - E$ .  $|M_{\Omega}(E)|^2$  is the  $\beta$ -decay strength function. The  $Q$  value represents the difference between the neutral atomic masses of parent and daughter nuclei, which can be written as  $Q = M(Z, A) - M(Z + 1, A)$ . The  $Q$  value is the most direct input for the calculation of the  $\beta$ -decay half-lives in the gross theory. In order to improve the accuracy, in this work, the masses of parent and daughter nuclei are derived from the WS4 mass model, which is one of the most accurate mass models at present. The integrated Fermi function  $f(Z, E_m)$  has usually been calculated with a phenomenological formula in the gross theory [16], which is a rough approximation, while in this work, it is improved to be

$$f(Z, E_m) = \frac{1}{m_e^5} \int_{m_e}^{E_m} p_e E_e (E_m - E_e)^2 F_0(Z + 1, E_e) dE_e, \quad (3)$$

where  $p_e$  and  $E_e$  are the emitted electron momentum and energy, respectively.  $F_0(Z, E_e)$  is the Fermi function including Coulomb screening and relativistic nuclear finite-size corrections. It can be calculated by

$$F_0(Z, E_e) = 2(1 + \gamma)(2p_e R)^{2(\gamma-1)} \left| \frac{\Gamma(\gamma + iy)}{\Gamma(2\gamma + 1)} \right|^2 e^{\pi y}, \quad (4)$$

with

$$\gamma = \sqrt{1 - (\alpha Z)^2} \quad \text{and} \quad y = \alpha Z E_e / p_e, \quad (5)$$

where  $R$  is the nuclear radius and  $\alpha$  is the fine-structure constant.

Using the sum rules and the gross approximation,  $|M_\Omega(E)|^2$  is defined as an appropriate average of the squared nuclear matrix elements times the final level density. The operation of the  $\beta$ -decay operator on a single nucleon with  $\varepsilon$  produces a contribution to  $|M_\Omega(E)|^2$  and this contribution is a single-particle strength function, i.e.,  $D_\Omega(E, \varepsilon)$ , which is the most basic assumption of the gross theory:

$$|M_\Omega(E)|^2 = \int_{\varepsilon_0(E)}^{\varepsilon_1} D_\Omega(E, \varepsilon) \frac{dn_1}{d\varepsilon} W(E, \varepsilon) d\varepsilon, \quad (6)$$

where  $dn_1/d\varepsilon$  is the single-particle energy distribution of the decaying nucleons determined by the Fermi gas model,  $\varepsilon_1$  is the maximum energy of the filled single-nucleon states, and  $\varepsilon_0(E) = \max(\varepsilon_{\min}, \varepsilon_1 - Q - E)$ , with  $\varepsilon_{\min}$  being the lowest single-particle energy of the parent nucleus. The Pauli principle is considered in the lower limit of the integral and in the term  $W(E, \varepsilon)$ , which is a weight function reflecting the availability (the degree of vacancy) of the final states. In the special case of the flat surface,  $W(E, \varepsilon)$  equals to unity for  $\varepsilon + E > \varepsilon_1 - Q$  and vanishes for  $\varepsilon + E \leq \varepsilon_1 - Q$ . As in Ref. [16], the dependence of the single-particle strength function  $D_\Omega(E, \varepsilon)$  on  $\varepsilon$  is neglected, i.e., suppose that each nucleon has the same decay potential, regardless of the energy  $\varepsilon$  of the nucleon,  $D_\Omega(E, \varepsilon) = D_\Omega(E)$ . The Fermi gas model is used to estimate the  $dn_1/d\varepsilon$  as

$$\frac{dn_1}{d\varepsilon} = \frac{2}{(2\pi\hbar)^3} 4\pi V [2M_n^{*3}(\varepsilon - \varepsilon_{\min})]^{1/2}, \quad \varepsilon_{\min} = \varepsilon_1 - \varepsilon_F, \quad (7)$$

where  $M_n^*$  is the effective nucleon masses.  $\varepsilon_F$  is the nucleon Fermi energy given by

$$\varepsilon_F = \frac{76.52}{(M_n^*/M_n)r_0^2} \left(\frac{N_1}{A}\right)^{2/3} \text{ MeV}, \quad (8)$$

where  $N_1$  is neutron number of the parent nuclei. For the nuclear radius  $R = r_0 A^{1/3}$ , we take  $r_0 = 1.2$ . Finally, the total  $\beta$ -decay rate can be written as

$$\lambda = \frac{m_e^5 c^4}{2\pi^3 \hbar^7} \int_{-Q}^0 \int_{\varepsilon_0(E)}^{\varepsilon_1} [G_F^2 D_F(E, \varepsilon) + 3G_{GT}^2 D_{GT}(E, \varepsilon)] \times \frac{dn_1}{d\varepsilon} W(E, \varepsilon) f(Z, E_m) d\varepsilon dE. \quad (9)$$

As in Ref. [16], the single-particle energy distribution  $dn_1/d\varepsilon$  and the single-particle strength function  $D_\Omega(E, \varepsilon)$  are

modified by the gap of the single-nucleon levels in the final nucleus to consider the pairing correlation.

## B. Single-particle strength function

The single-particle strength function is constructed based on the sum rule and the energy-weighted sum rules, and it usually takes the Gaussian form as follows:

$$D_\Omega(E) = \frac{1}{\sqrt{2\pi}\sigma_\Omega} \exp\left\{-\frac{(E - \Delta_\Omega)^2}{2\sigma_\Omega^2}\right\}, \quad (10)$$

where  $\Delta_\Omega$  and  $\sigma_\Omega$  are the resonance energy and the standard deviation. In the case of the Gamow-Teller transition, which is the dominant nuclear process in  $\beta$  decay, the sum rules are [61] as follows:

$$\int_{-\infty}^{\infty} D_{GT}(E) dE = 1, \quad (11)$$

$$\int_{-\infty}^{\infty} E D_{GT}(E) dE \approx \Delta_{GT}, \quad (12)$$

$$\int_{-\infty}^{\infty} (E - \Delta_{GT})^2 D_{GT}(E) dE \approx \sigma_{GT}^2, \quad (13)$$

which determine the amplitude, the expectation, and the standard deviation of the single-particle strength function, respectively. As in Ref. [16], the nucleus is assumed to be a uniformly charged sphere of radius  $1.2A^{1/3}$  fm, and we get the following for  $\beta^\pm$  decay,

$$\Delta_F = \Delta_C = \mp(1.44Z_1 A^{-1/3} - 0.7825) \text{ MeV}, \quad (14)$$

$$\sigma_F = \sigma_C = 0.157Z_1 A^{-1/3} \text{ MeV}, \quad (15)$$

where  $Z_1$  is the proton number of the daughter nucleus for  $\beta^+$  decay and that of the parent one for  $\beta^-$  decay. Here  $\Delta_C$  and  $\sigma_C$  are the single-particle Coulomb displacement and the fluctuation (or the standard deviation) of the Coulomb energy [16]. The standard deviation of the Gamow-Teller transition is calculated with

$$\sigma_{GT}^2 = \sigma_F^2 + \sigma_N^2, \quad (16)$$

where  $\sigma_N$  is the energy spread caused by the spin-dependent part of nuclear forces.

The central energy of the Gamow-Teller transition  $\Delta_{GT}$  is certainly different from that of the Fermi transition  $\Delta_F$ , while it is usually taken as  $\Delta_{GT} = \Delta_F$  for simplicity in the original gross theory [16]. From Refs. [62,63], the relationship between  $\Delta_{GT}$  and  $\Delta_F$  can be calculated with

$$\Delta_{GT} - \Delta_F = \frac{1}{8(N-Z)} \left\langle \pi \left| \left[ \sum_i^A \tau_+^i \sigma_+^i, \left[ H_1, \sum_j^A \tau_-^j \sigma_-^j \right] \right] \right| \pi \right\rangle, \quad (17)$$

where  $|\pi\rangle$  represent the parent nucleus.  $H_1$  stands for the spin-dependent, isospin-dependent, and spin-isospin-dependent parts of the Hamiltonian used in Ref. [62]; it can be expressed as

$$H_1 = - \sum_{i=1}^A \xi_i \mathbf{l}_i \cdot \boldsymbol{\sigma}_i + \frac{1}{2} \frac{\kappa_\tau}{A} \sum_{i \neq j}^A \boldsymbol{\tau}_i \cdot \boldsymbol{\tau}_j + \frac{1}{2} \frac{\kappa_\sigma}{A} \sum_{i \neq j}^A \boldsymbol{\sigma}_i \cdot \boldsymbol{\sigma}_j + \frac{1}{2} \frac{\kappa_{\sigma\tau}}{A} \sum_{i \neq j}^A (\boldsymbol{\tau}_i \cdot \boldsymbol{\tau}_j)(\boldsymbol{\sigma}_i \cdot \boldsymbol{\sigma}_j), \quad (18)$$

where  $\kappa_\tau$  and  $\kappa_{\sigma\tau}$  are the strengths of the isospin-dependent and spin-isospin-dependent interactions, respectively.  $\xi_i$  and  $l_i$  are the strength of the  $l \cdot \sigma$  force and the orbital angular momentum. The average energy difference between Gamow-Teller and Fermi transitions can then be obtained by using the Hamiltonian  $H_1$  with the  $\xi l \cdot \sigma$  force, which is

$$\begin{aligned} \Delta_{\text{GT}} - \Delta_{\text{F}} &= \frac{2}{3T_0} \left\langle \pi \left| \sum_{i=1}^A \xi_i l_i \cdot \sigma_i \right| \pi \right\rangle - 4A^{-1}(\kappa_\tau - \kappa_{\sigma\tau})T_0 \\ &= \Delta_{I_s} - 4A^{-1}(\kappa_\tau - \kappa_{\sigma\tau})T_0. \end{aligned} \quad (19)$$

Here  $T_0 = (N - Z)/2$  represents the total isospin.  $\Delta_{I_s}$  comes from the  $l \cdot \sigma$  force, reflecting the fact that particle-hole states composed of spin-orbit partners contribute to the Gamow-Teller modes. This formula can also be understood from the QRPA calculations. It is known that the main configurations of the Gamow-Teller resonance are the transitions of type  $j = l + 1/2 \rightarrow j = l - 1/2$  ( $j$  is the total angular momentum and  $l$  is the orbital angular momentum of the upper component), while the configurations of the Fermi transition are the transitions of type  $j = l \pm 1/2 \rightarrow j = l \pm 1/2$ . Therefore, the differences between the unperturbed energies of the Gamow-Teller resonance and those of the Fermi transition can be roughly estimated by  $\Delta_{I_s}$ . Apart from the differences between the unperturbed energies, the influence of residual interactions on  $\Delta_{\text{GT}} - \Delta_{\text{F}}$  is certainly important, which is simulated by the second term of Eq. (19), since this term is proportional to the difference between the strengths of spin-isospin-dependent and isospin-dependent interactions.

### C. Model parameters

Similarly as in Refs. [62–64], in this work,  $\Delta_{\text{GT}}$  is calculated by

$$\Delta_{\text{GT}} = \Delta_{\text{F}} + \Delta_{I_s} + \Delta_\kappa, \quad (20)$$

with

$$\Delta_{I_s} = \frac{2}{3(N - Z)} E_{I_s}, \quad \Delta_\kappa = 2(\kappa_{\sigma\tau} - \kappa_\tau)(N - Z)/A, \quad (21)$$

where  $\Delta_{I_s}$  is the contribution of spin-orbit splitting to  $\Delta_{\text{GT}} - \Delta_{\text{F}}$  as derived from Refs. [62,63]. The average spin-orbit splitting  $E_{I_s}$  is extracted from the single-particle levels of the RHB theory with PC-PK1 [65] for each nucleus, while in previous versions of the gross theory it is taken as a constant [17] or a phenomenological formula only depending on  $A$  [66,67]. In the QRPA calculations, the occupation ( $v^2$ ) and unoccupation ( $u^2 = 1 - v^2$ ) probabilities of single-particle levels in the canonical basis should be further included [68]. Therefore, the single-particle levels and the occupation probabilities of the RHB theory in the canonical basis are employed to extract the average spin-orbit splitting, which is calculated by

$$E_{I_s} = \sum_i \frac{\Delta E_i [(u_{p^-}^2 v_{n^+}^2) \mu_{p^-} \mu_{n^+} - (u_{p^+}^2 v_{n^-}^2) \mu_{p^+} \mu_{n^-}]_i}{2l_i + 1}, \quad (22)$$

where  $\mu = 2j + 1$  is the degeneracy of the single-particle level. Both the neutron and the proton energy levels used here belong to the parent nucleus.  $p^\pm$  ( $n^\pm$ ) are the single proton (neutron) states with the opposite spin  $j = l \pm 1/2$ .

The summation on  $i$  runs over all spin-orbit partners and  $\Delta E_i$  is their spin-orbit splitting for proton energy levels. The reason for it is that we assume that the energy difference of the spin-orbit partners is the same for neutrons and protons. When the pairing correlation is switched off, Eq. (22) clearly becomes the average spin-orbit splitting among spin-orbit partners of (neutron) particle-(proton) hole pairs. Taking the closed-shell nucleus  $^{48}\text{Ca}$  as an example, whose protons occupy the major shells and  $N - Z = 8$  neutrons fill the  $j = l + 1/2$  ( $1f_{7/2}$ ) shell, only the spin-orbit partners ( $1f_{7/2}$ ,  $1f_{5/2}$ ) can contribute the average spin-orbit splitting in Eq. (22). Therefore,  $E_{I_s}(^{48}\text{Ca}) = 48\Delta E_{1f}/7$  and hence the  $\Delta_{I_s}(^{48}\text{Ca})$  in Eq. (21) equals  $2E_{I_s}(^{48}\text{Ca})/24 = 4\Delta E_{1f}/7$ . For  $^{208}\text{Pb}$ , whose protons occupy up to the  $1h_{11/2}$  shell and neutrons up to the  $1i_{13/2}$  shell, the contributions from the spin-orbit partners ( $2f_{7/2}$ ,  $2f_{5/2}$ ) and ( $3p_{3/2}$ ,  $3p_{1/2}$ ) cancel out, so only the remaining partners ( $1h_{11/2}$ ,  $1h_{9/2}$ ) and ( $1i_{13/2}$ ,  $1i_{11/2}$ ) can contribute the average spin-orbit splitting. Therefore,  $E_{I_s}(^{208}\text{Pb}) = 120\Delta E_{1h}/11 + 168\Delta E_{1i}/13$  and hence  $\Delta_{I_s}(^{208}\text{Pb})$  equals  $2E_{I_s}(^{208}\text{Pb})/132 = 4(5\Delta E_{1h}/11 + 7\Delta E_{1i}/13)/11$ . These results are consistent with the formulas  $\Delta_{I_s}(^{48}\text{Ca}) = 4\xi_3$  and  $\Delta_{I_s}(^{208}\text{Pb}) = 4(5\xi_5 + 7\xi_6)/11$  in Refs. [62,63] by using  $\xi_l = \Delta E_l/(2l + 1)$ . Therefore, we use Eq. (22) to extract the average spin-orbit splitting.

Clearly, there are only two independent parameters in this gross theory, i.e.,  $\sigma_N$  and  $(\kappa_{\sigma\tau} - \kappa_\tau)$ . The parameter  $(\kappa_{\sigma\tau} - \kappa_\tau)$  is determined by fitting the experimental difference between the central energies of the Gamow-Teller and the Fermi transitions of Zr, Sn, and Pb isotopes [69–71], which is  $-4.8765$  MeV. Using the least-square method, the optimal value of the last remaining parameter  $\sigma_N$  is obtained by fitting the experimental  $\beta$ -decay half-lives to minimize

$$S = \sum_{n=1}^{N_0} [\log_{10}(T_{1/2}^{\text{cal}}(n)/T_{1/2}^{\text{exp}}(n))]^2, \quad (23)$$

where  $n$  represents the  $n$ th nucleus and  $N_0$  is the total number of nuclei. In principle, the parameter  $\sigma_N$  should be refitted for the gross theory with  $Q$  values from other mass models, while it is very similar for most nuclear mass models, so we adopt the value of  $\sigma_N$  in the gross theory based on the WS4 mass model for the gross theory based on the KTUY mass model, which is 7.6996 MeV.

The direct inputs for calculating the  $\beta$ -decay half-life are the proton number  $Z$ , the neutron number  $N$ , and the  $\beta$ -decay-energy  $Q$  value. In this work, the  $\beta$ -decay-energy  $Q$  values are provided by the WS4 mass model, whose root-mean-square (rms) deviation to the latest experimental mass evaluation AME2020 [72] is about 300 keV, even better than that in the SHFB [42] and FRDM12 [47] mass models. For simplicity, the improved gross theory is referred to as the WS4+GT model hereafter. In order to give better descriptions of nuclear half-lives,  $\sigma_N$  is refitted with experimental half-lives NUBASE2016 [73], in which only nuclei with  $T_{1/2} < 100$  s and decaying 100% by the  $\beta$  mode are considered. In addition,  $\Delta_{\text{GT}}$  is improved by including the spin-orbit corrections and the term of  $(\kappa_{\sigma\tau} - \kappa_\tau)$  in this work. Since the experimental  $\Delta_{\text{GT}} - \Delta_{\text{F}}$  can be well reproduced, the spin-orbit corrections and the term of  $(\kappa_{\sigma\tau} - \kappa_\tau)$  can be used for all gross theories,

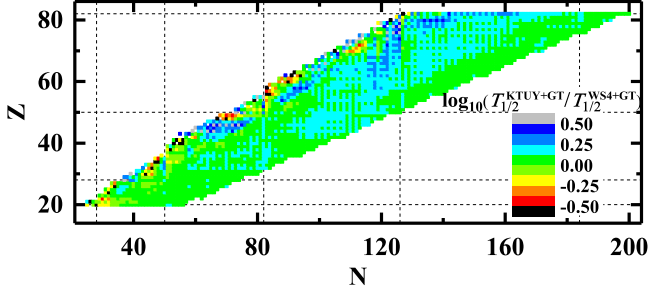


FIG. 1. Differences of  $\log_{10}(T_{1/2})$  between KTUY+GT and WS4+GT predictions.

not only for the one based on the WS4 mass model. Therefore, it is possible the WS4+GT model is better able to reproduce the real physics and hence better able to describe nuclear  $\beta$ -decay half-lives.

### III. RESULTS AND DISCUSSION

From Eq. (2), it is clear that the  $Q$  value and the integrated Fermi function  $f$  play important roles in predictions of nuclear  $\beta$ -decay half-lives. By taking the KTUY and WS4 mass models as examples, Figure 1 shows the logarithmic difference of the  $\beta$ -decay half-lives obtained using different  $Q$  values from these two mass models. It can be seen that the differences between the predicted  $\log_{10}(T_{1/2})$  of KTUY+GT and WS4+GT generally become smaller and smaller when moving towards the neutron drip line. In the very neutron-rich region, the logarithmic differences of  $\beta$ -decay half-lives of the two models are generally within 0.25, while these differences are even larger than 0.5 for nuclei near the stability line. These large differences for nuclei near the stability line can be understood by their very small  $Q$  values and hence minor changes in their  $Q$  values would induce large changes in half-lives. Figure 2 shows the comparison between the half-life calculations with the approximate integrated Fermi function in Ref. [16] and the improved integrated Fermi function in Eq. (3). Clearly, the approximate integrated Fermi function widely used in the gross theory is very accurate in the very neutron-rich region and the light nuclei region with  $Z \lesssim 70$ . However, for heavy nuclei with  $Z \gtrsim 70$  near the stability line,

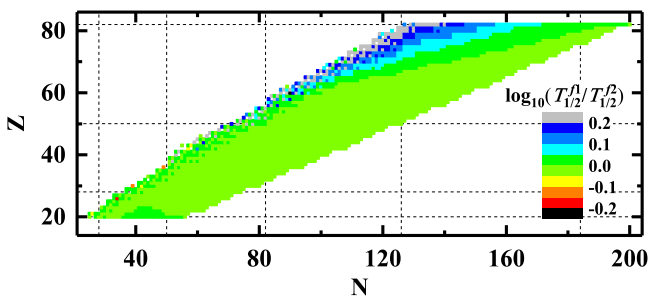


FIG. 2. Differences between  $\log_{10}(T_{1/2})$  obtained using two different integrated Fermi functions. The superscripts  $f1$  and  $f2$  represent the approximate integrated Fermi function in Ref. [16] and the improved integrated Fermi function in Eq. (3), respectively.

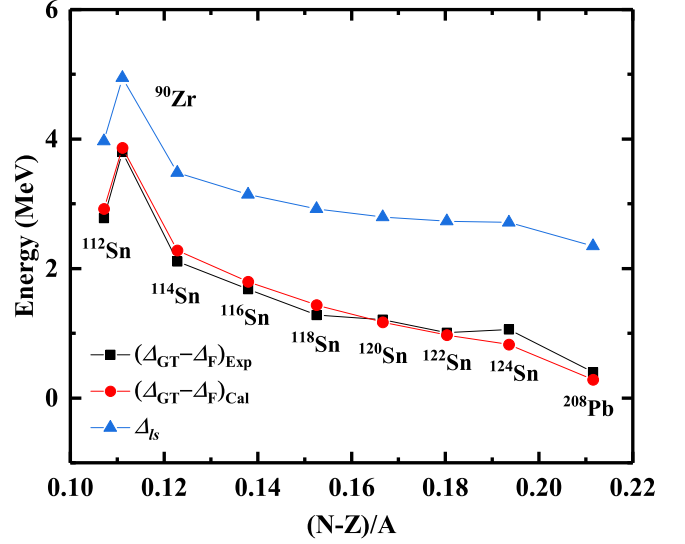


FIG. 3. The differences between the central energies of the Gamow-Teller and the Fermi transitions for Zr, Sn, and Pb isotopes. The corresponding experimental data [69–71] and theoretical results are denoted by circles and squares, respectively. For comparison, the spin-orbit splitting term  $\Delta_{Is}$  is denoted by triangles.

large differences in the integrated Fermi function are found and hence induce systematic deviations of half-life predictions. Therefore, it is necessary to adopt more accurate  $Q$  values and integrated Fermi functions, and we use  $Q$  values from the WS4 mass model and the integrated Fermi function in Eq. (3) to predict nuclear  $\beta$ -decay half-lives hereafter. Figure 3 shows the differences between the central energies of the Gamow-Teller and the Fermi transitions ( $\Delta_{GT} - \Delta_F$ ) as a function of isospin  $(N - Z)/A$ . The contribution from the spin-orbit splitting term  $\Delta_{Is}$  is shown as well. It is found that  $\Delta_{Is}$  plays a key role in describing the experimental  $\Delta_{GT} - \Delta_F$ , such as the abrupt increase and decrease at  $^{90}\text{Zr}$  and  $^{208}\text{Pb}$ . The interaction term  $\Delta_{\kappa}$  provides the main decreasing trend of  $(\Delta_{GT} - \Delta_F)$  with the isospin, which is also important to reproduce the absolute value of  $\Delta_{GT} - \Delta_F$ . From Fig. 3, the predicted differences between the central energies of the Gamow-Teller and Fermi transitions by Eq. (20) are in excellent agreement with experimental data in a large range of isospins from about 0.1 to about 0.22. In order to investigate the evolution of the central energies of Fermi and Gamow-Teller transitions as a function of neutron number, and the contributions from the spin-orbit coupling term  $\Delta_{Is}$ , the central energies of the Gamow-Teller and Fermi transitions for Ni and Sn isotopes are shown in Fig. 4 as well as  $\Delta_{Is}$ . The  $\Delta_{Is}$  value slowly decreases with the increasing of the neutron number, while its change becomes slower and even slightly increases when the neutron number approaches the magic numbers 50 and 82. This also demonstrates again the importance of the interaction term  $\Delta_{\kappa}$ , that is, providing the downward trend of the Gamow-Teller transition central energy  $\Delta_{GT}$  with the number of neutrons  $N$ . The Fermi transition central energy is mainly related to the nuclear proton number, so its change is small in one isotopic chain, which is only about 1 MeV for Ni isotopes and 1.5 MeV for Sn

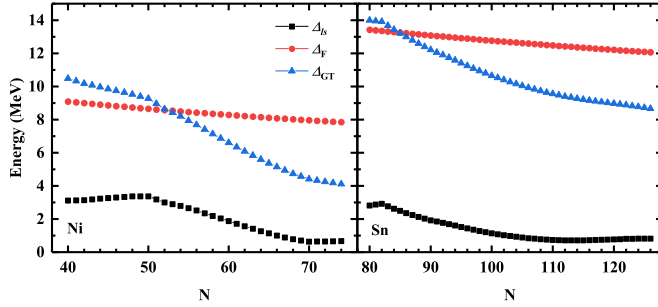


FIG. 4. Central energies of the Fermi transition and the Gamow-Teller transition, and the average value of spin-orbit splitting for Ni and Sn isotopes.

isotopes. However, the change of the Gamow-Teller transition central energy is very large, which is about 6.4 MeV for Ni isotopes and 5.3 MeV for Sn isotopes. These energy reductions are further checked with the corresponding QRPA calculations with SkM\*. From the QRPA calculations, it is found that the Gamow-Teller transition energies are reduced by 8.2 MeV (from 10.0 MeV of  $^{68}\text{Ni}$  to 1.8 MeV of  $^{102}\text{Ni}$ ) and 7.1 MeV (from 12.3 MeV of  $^{130}\text{Sn}$  to 5.2 MeV of  $^{176}\text{Sn}$ ) for Ni and Sn isotopes, which supports the decreasing trend of Gamow-Teller transition central energy with the neutron number towards the neutron drip line in Fig. 4. Therefore, it is necessary to consider the differences between the Gamow-Teller and Fermi transition central energies. The effect of different Gamow-Teller transition central energies  $\Delta_{GT}$  on the nuclear half-lives was further investigated. Taking the Ni and Sn isotopes as examples, their half-lives are shown in Fig. 5. Compared with the results with  $\Delta_{GT} = \Delta_F$ , the inclusion of the interaction term  $\Delta_k$  reduces the predicted  $\beta$ -decay half-lives, and its influence becomes larger and larger as the neutron number is increased. By further including the  $\Delta_{I_s}$  term in the calculations of  $\Delta_{GT}$ , the underestimate of half-lives is effectively eliminated and hence can well reproduce the experimental half-lives. From Fig. 4, it is found that  $\Delta_{GT}$  values of Ni (Sn) isotopes are larger than  $\Delta_F$  values when  $N < 53$  ( $N < 85$ ), so their half-lives would increase by including the differences between  $\Delta_{GT}$  and  $\Delta_F$ , but this influence on half-lives is not obvious from Fig. 5. Thus, a good description of half-lives can also be obtained using  $\Delta_{GT} = \Delta_F$  in the known

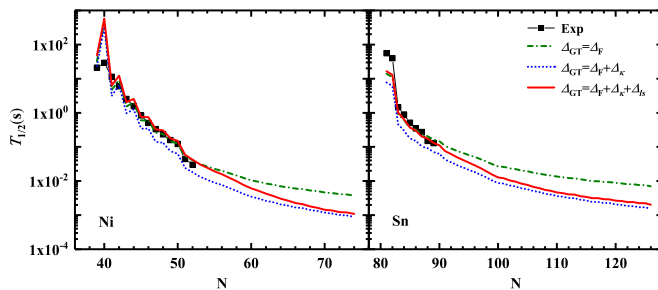


FIG. 5. Nuclear  $\beta$ -decay half-lives of Ni and Sn isotopes. The dot-dashed, dotted, and solid lines represent the half-lives with  $\Delta_{GT} = \Delta_F$ ,  $\Delta_{GT} = \Delta_F + \Delta_k$ , and  $\Delta_{GT} = \Delta_F + \Delta_k + \Delta_{I_s}$ , respectively. The experimental values are denoted by solid squares.

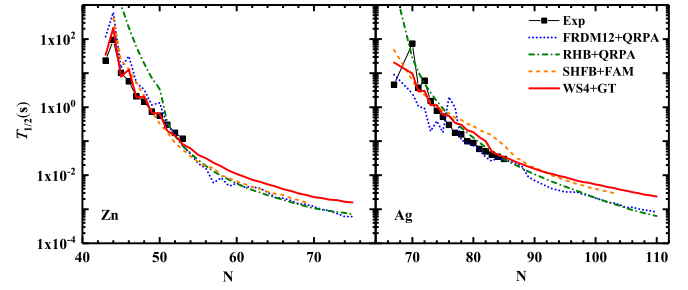
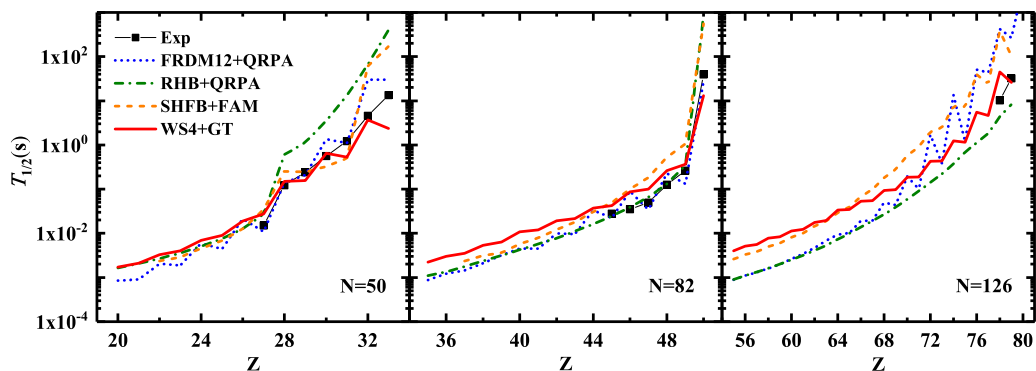


FIG. 6.  $\beta$ -decay half-lives of Zn and Ag isotopes. The results of the WS4+GT, RHB+QRPA [31], FRDM12+QRPA [32], and SHFB+FAM [36] models are shown with solid, dot-dashed, dotted, and dashed lines, respectively. For comparison, the experimental data are shown with solid squares.

region for the early version of the gross theory. However, this influence becomes larger and larger when extrapolating towards neutron drip-line nuclei and even approaches an order of magnitude. Therefore, it is necessary to consider the differences between the Gamow-Teller and Fermi transition central energies for better describing  $\beta$ -decay half-lives of nuclei from near the stability line to the neutron drip line. For comparison with experimental and other models' results, e.g., the QRPA methods based on the FRDM (FRDM12+QRPA) [32] and the RHB theory (RHB+QRPA) [31], as well as the FAM based on the SHFB theory (SHFB+FAM) [36], we take even- $Z$  Zn and odd- $Z$  Ag isotopes as examples, whose half-lives are shown in Fig. 6. For Zn isotopes, the FRDM12+QRPA and RHB+QRPA models overestimate nuclear  $\beta$ -decay half-lives for those with  $N < 50$ , while the WS4+GT and SHFB+FAM models well reproduce all known half-lives. For Ag isotopes, WS4+GT and RHB+QRPA models well reproduce the known  $\beta$ -decay half-lives, while the FRDM12+QRPA model generally underestimates the half-lives of long-lived nuclei ( $T_{1/2} \gtrsim 1$  s) and SHFB+FAM model overestimates the half-lives of short-lived nuclei ( $T_{1/2} \lesssim 1$  s). When extrapolating to the very neutron-rich region, the half-lives predicted by the WS4+GT model are systematically larger than those of the FRDM12+QRPA and RHB+QRPA models and are close to those of the SHFB+FAM model, especially for the Ag isotopes. The RHB+QRPA model usually predicts shorter half-lives for very neutron-rich nuclei, this may originate from the inclusion of isoscalar proton-neutron pairing interaction, whose strength becomes larger for these neutron-rich nuclei. In addition, the half-lives of  $N = 50, 82,$  and  $126$  isotones, which are important for  $r$ -process nucleosynthesis, are investigated, and the results are shown in Fig. 7. For  $N = 50$  isotones, the RHB+QRPA [31] model overestimates the experimental half-lives when  $Z > 28$ . The WS4+GT model underestimates the half-lives of  $N = 50$  isotones with odd  $Z$ , but it describes well the half-lives of  $N = 50$  isotones with even  $Z$ . Therefore, the WS4+GT model predicts an odd-even staggering of half-lives for  $N = 50$  isotones in the known region, while it becomes very weak when  $Z < 27$ . This odd-even staggering is also remarkable in FRDM12+QRPA [32] predictions, even extrapolating to the unknown neutron-rich region. For the  $N = 82$  isotones,

FIG. 7. Same as Fig. 6, but for  $N = 50, 82,$  and  $126$  isotones.

the WS4+GT and RHB+QRPA models better reproduce the experimental data, while the SHFB+FAM [36] model systematically overestimates the known half-lives. For the odd-even staggering of half-lives of  $N = 82$  isotones, it is already very weak even in the known region for the WS4+GT model, while it is still remarkable for the FRDM12+QRPA model. For  $N = 126$  isotones, the RHB+QRPA model does not show the odd-even staggering phenomenon, but remarkably underestimates the known half-lives, which may be due to the large strength of isoscalar proton-neutron pairing interaction. Both the FRDM12+QRPA and SHFB+FAM models overestimate the known half-lives, while the WS4+GT model better reproduces the experimental data. The odd-even staggering of half-lives for SHFB+FAM and WS4+GT models is much weaker than that for the FRDM12+QRPA model. The odd-even staggering of half-lives can be related to the odd-even staggering of  $Q$  values, so it is very important to construct a reliable strength function to weaken or eliminate the odd-even staggering of half-lives. The weak odd-even staggering of half-lives for the RHB+QRPA and SHFB+FAM models may indicate the self-consistency of the model plays an important role in getting reliable strength functions. From the above discussions, it is clear that the WS4+GT model can well describe nuclear  $\beta$ -decay half-lives not only for the even- $Z$  and odd- $Z$  isotopes but also for the isotones. The  $\beta$ -decay

half-lives are then systematically calculated for the neutron-rich nuclei from Ca to Pb isotopes by using the WS4+GT model, whose data table is available as the Supplemental Material [74]. For comparison with the experimental data, the differences of  $\log_{10}(T_{1/2})$  between WS4+GT predictions and experimental data are shown in Fig. 8. The WS4+GT model better describes nuclear  $\beta$ -decay half-lives, and the differences of  $\log_{10}(T_{1/2})$  between the experimental half-lives and the WS4+GT predictions are generally within  $0.5$  ( $10^{0.5} = 3.2$  times), which further verifies the reliability of the  $\beta$ -decay half-lives predicted by the WS4+GT model. This improvement in the half-life accuracy can also be reflected from the rms deviations of  $\log_{10}(T_{1/2})$ ; the corresponding rms values of the WS4+GT, SHFB+FAM [36], RHB+QRPA [31], and FRDM12+QRPA [32] models for nuclei with experimental  $T_{1/2} < 100$  s are 0.40, 0.62, 0.80, and 0.53, respectively. The very large values of predicted half-lives ( $T_{1/2} > 10^6$  s) are excluded in the rms calculation of the RHB+QRPA model in order to get a reasonable evaluation of its half-life accuracy. Finally, as shown in Fig. 9, the WS4+GT predictions are

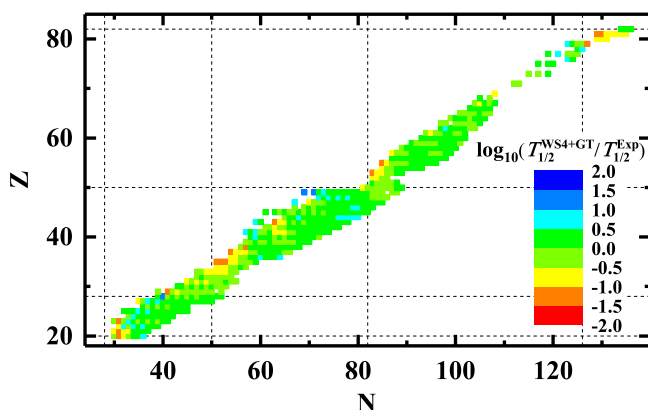
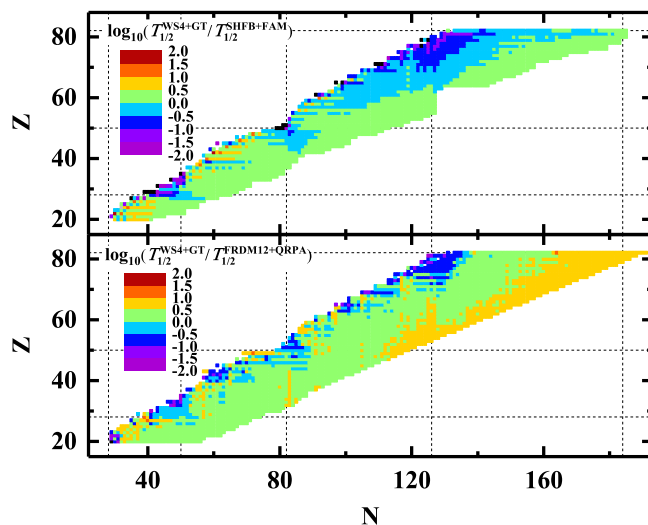
FIG. 8. Differences of  $\log_{10}(T_{1/2})$  between WS4+GT predictions and experimental data.

FIG. 9. Logarithmic values for the comparison of WS4+GT predictions with SHFB+FAM [36] and FRDM12+QRPA [32] predictions.

compared with the SHFB+FAM and FRDM12+QRPA predictions, respectively. The WS4+GT predictions are generally closer to those of the SHFB+FAM model, especially in the very neutron-rich region without experimental data. The corresponding  $\sigma_{\text{rms}}$  of  $\log_{10}(T_{1/2})$  between WS4+GT predictions and SHFB+FAM (FRDM12+QRPA) predictions is only 0.45 (0.46), which shows their half-life predictions are generally within about 3 times.

#### IV. SUMMARY

In summary, the gross theory for predicting nuclear  $\beta$ -decay half-lives is improved by employing more reliable Gamow-Teller transition central energies. In this treatment, the Gamow-Teller transition central energies include the interaction term and the spin-orbit coupling term, which are found to be very important for reproducing the experimental data. The influence of the  $Q$  value from different mass models on the calculations of  $\beta$ -decay half-lives is studied with an improved integrated Fermi function. Based on the mass predictions of the WS4 model and the spin-orbit splitting

extracted from the relativistic Hartree-Bogoliubov theory, the gross theory is employed to systematically calculate nuclear  $\beta$ -decay half-lives for neutron-rich nuclei from Ca to Pb isotopes. The effects of the interaction term and the spin-orbit coupling term on the  $\beta$ -decay half-lives are also investigated in detail. By comparing with microscopic SHFB+FAM, RHB+QRPA, and FRDM12+QRPA models, the WS4+GT model better reproduces known  $\beta$ -decay half-lives, whose rms deviation of  $\log_{10}(T_{1/2})$  is only 0.4 ( $10^{0.4} = 2.5$  times) for nuclei with experimental  $T_{1/2} < 100$  s. When extrapolated to the unknown neutron-rich region, the WS4+GT predictions are generally close to the SHFB+FAM predictions.

#### ACKNOWLEDGMENTS

This work was partly supported by the National Natural Science Foundation of China under Grants No. 11875070 and No. 11935001 and by the Anhui project (Grant No. Z010118169). The authors acknowledge the High-performance Computing Platform of Anhui University for providing computing resources.

- 
- [1] F. G. Kondev, M. Wang, W. J. Huang, S. Naimi, and G. Audi, *Chin. Phys. C* **45**, 030001 (2021).
- [2] D. Lunney, J. M. Pearson, and C. Thibault, *Rev. Mod. Phys.* **75**, 1021 (2003).
- [3] E. Nacher, A. Algora, B. Rubio, J. L. Tain, D. Cano-Ott, S. Courtin *et al.*, *Phys. Rev. Lett.* **92**, 232501 (2004).
- [4] V. Tripathi, S. L. Tabor, P. F. Mantica, Y. Utsuno, P. Bender, J. Cook *et al.*, *Phys. Rev. Lett.* **101**, 142504 (2008).
- [5] O. Sorlin, D. Guillemaud-Mueller, A. C. Mueller, V. Borrel, S. Dognny, F. Pougheon *et al.*, *Phys. Rev. C* **47**, 2941 (1993).
- [6] E. M. Burbidge, G. R. Burbidge, W. A. Fowler, and F. Hoyle, *Rev. Mod. Phys.* **29**, 547 (1957).
- [7] T. Kajino, W. Aoki, A. B. Balantekin, R. Diehl, M. A. Famiano, and G. J. Mathews, *Prog. Part. Nucl. Phys.* **107**, 109 (2019).
- [8] J. J. Cowan, C. Sneden, J. E. Lawler, A. Aprahamian, M. Wiescher, K. Langanke, G. Martínez-Pinedo, and F. K. Thielemann, *Rev. Mod. Phys.* **93**, 015002 (2021).
- [9] Z. Li, Z. M. Niu, and B. H. Sun, *Sci. China Phys. Mech. Astron.* **62**, 982011 (2019).
- [10] G. Lorusso *et al.*, *Phys. Rev. Lett.* **114**, 192501 (2015).
- [11] J. Wu, S. Nishimura, P. Möller *et al.*, *Phys. Rev. C* **101**, 042801 (2020).
- [12] J. Wu, S. Nishimura, G. Lorusso *et al.*, *Phys. Rev. Lett.* **118**, 072701 (2017).
- [13] T. Kurtukian-Nieto *et al.*, *Eur. Phys. J. A* **50**, 135 (2014).
- [14] Y. Zhou, Z. H. Li, Y. B. Wang *et al.*, *Sci. China Phys. Mech. Astron.* **60**, 082012 (2017).
- [15] M. Shi, J. Y. Fang, and Z. M. Niu, *Chin. Phys. C* **45**, 044103 (2021).
- [16] K. Takahashi and M. Yamada, *Prog. Theor. Phys.* **41**, 1470 (1969).
- [17] T. Tachibana, M. Yamada, and Y. Yoshida, *Prog. Theor. Phys.* **84**, 641 (1990).
- [18] H. Nakata, T. Tachibana, and M. Yamada, *Nucl. Phys. A* **625**, 521 (1997).
- [19] H. Koura and S. Chiba, *Phys. Rev. C* **95**, 064304 (2017).
- [20] J. Engel, M. Bender, J. Dobaczewski, W. Nazarewicz, and R. Surman, *Phys. Rev. C* **60**, 014302 (1999).
- [21] F. Minato and C. L. Bai, *Phys. Rev. Lett.* **110**, 122501 (2013).
- [22] Z. M. Niu, Y. F. Niu, H. Z. Liang, W. H. Long, and J. Meng, *Phys. Rev. C* **95**, 044301 (2017).
- [23] I. N. Borzov and S. Goriely, *Phys. Rev. C* **62**, 035501 (2000).
- [24] K. Langanke and G. Martínez-Pinedo, *Rev. Mod. Phys.* **75**, 819 (2003).
- [25] G. Martínez-Pinedo and K. Langanke, *Phys. Rev. Lett.* **83**, 4502 (1999).
- [26] T. Suzuki, T. Yoshida, T. Kajino, and T. Otsuka, *Phys. Rev. C* **85**, 015802 (2012).
- [27] Q. Zhi, E. Caurier, J. J. Cuenca-García, K. Langanke, G. Martínez-Pinedo, and K. Sieja, *Phys. Rev. C* **87**, 025803 (2013).
- [28] Z. M. Niu, Y. F. Niu, H. Z. Liang, W. H. Long, T. Nikšić, D. Vretenar, and J. Meng, *Phys. Lett. B* **723**, 172 (2013).
- [29] Z. M. Niu, Y. F. Niu, Q. Liu, H. Z. Liang, and J. Y. Guo, *Phys. Rev. C* **87**, 051303(R) (2013).
- [30] Z. Y. Wang, Y. F. Niu, Z. M. Niu, and J. Y. Guo, *J. Phys. G: Nucl. Part. Phys.* **43**, 045108 (2016).
- [31] T. Marketin, L. Huther, and G. Martínez-Pinedo, *Phys. Rev. C* **93**, 025805 (2016).
- [32] P. Möller, M. R. Mumpower, T. Kawano, and W. D. Myers, *At. Data Nucl. Data Tables* **125**, 1 (2019).
- [33] T. Nakatsukasa, T. Inakura, and K. Yabana, *Phys. Rev. C* **76**, 024318 (2007).
- [34] H. Liang, T. Nakatsukasa, Z. Niu, and J. Meng, *Phys. Rev. C* **87**, 054310 (2013).
- [35] M. T. Mustonen and J. Engel, *Phys. Rev. C* **93**, 014304 (2016).
- [36] E. M. Ney, J. Engel, T. Li, and N. Schunck, *Phys. Rev. C* **102**, 034326 (2020).
- [37] S. Koyama, K. Takahashi, and M. Yamada, *Prog. Theor. Phys.* **44**, 663 (1970).
- [38] K. Takahashi, *Prog. Theor. Phys.* **45**, 1466 (1971).
- [39] F. Endo and H. Koura, *Phys. Rev. C* **99**, 034303 (2019).



- [40] D. N. Possidonio, R. C. Ferreira, A. J. Dimarco, C. A. Barbero, A. R. Samana, M. R. Azevedo, C. L. Santana, and A. E. Mariano, *Braz. J. Phys.* **48**, 485 (2018).
- [41] M. R. Azevedo, R. C. Ferreira, A. J. Dimarco, C. A. Barbero, A. R. Samana, and D. N. Possidonio, *Braz. J. Phys.* **50**, 57 (2020).
- [42] S. Goriely, N. Chamel, and J. M. Pearson, *Phys. Rev. Lett.* **102**, 152503 (2009).
- [43] S. Goriely, S. Hilaire, M. Girod, and S. Péru, *Phys. Rev. Lett.* **102**, 242501 (2009).
- [44] L. S. Geng, H. Toki, and J. Meng, *Prog. Theor. Phys.* **113**, 785 (2005).
- [45] X. M. Hua, T. H. Heng, Z. M. Niu, B. H. Sun, and J. Y. Guo, *Sci. China Phys. Mech. Astron.* **55**, 2414 (2012).
- [46] Q. S. Zhang, Z. M. Niu, Z. P. Li, J. M. Yao, and J. Meng, *Front. Phys.* **9**, 529 (2014).
- [47] P. Möller, W. D. Myers, H. Sagawa, and S. Yoshida, *Phys. Rev. Lett.* **108**, 052501 (2012).
- [48] N. Wang, M. Liu, X. Z. Wu, and J. Meng, *Phys. Lett. B* **734**, 215 (2014).
- [49] H. Koura, T. Tachibana, M. Uno, and M. Yamada, *Prog. Theor. Phys.* **113**, 305 (2005).
- [50] I. O. Morales, P. Van Isacker, V. Velázquez, J. Barea, J. Mendoza-Temis, J. C. López Vieyra, J. G. Hirsch, and A. Frank, *Phys. Rev. C* **81**, 024304 (2010).
- [51] Z. M. Niu, Z. L. Zhu, Y. F. Niu, B. H. Sun, T. H. Heng, and J. Y. Guo, *Phys. Rev. C* **88**, 024325 (2013).
- [52] Z. M. Niu, B. H. Sun, H. Z. Liang, Y. F. Niu, and J. Y. Guo, *Phys. Rev. C* **94**, 054315 (2016).
- [53] R. Utama, J. Piekarewicz, and H. B. Prosper, *Phys. Rev. C* **93**, 014311 (2016).
- [54] Z. M. Niu and H. Z. Liang, *Phys. Lett. B* **778**, 48 (2018).
- [55] Z. M. Niu, J. Y. Fang, and Y. F. Niu, *Phys. Rev. C* **100**, 054311 (2019).
- [56] J. Meng, H. Toki, S. G. Zhou, S. Q. Zhang, W. H. Long, and L. S. Geng, *Prog. Part. Nucl. Phys.* **57**, 470 (2006).
- [57] D. Vretenar, A. V. Afanasjev, G. A. Lalazissis, and P. Ring, *Phys. Rep.* **409**, 101 (2005).
- [58] T. Nikšić, D. Vretenar, P. Finelli, and P. Ring, *Phys. Rev. C* **66**, 024306 (2002).
- [59] S. G. Zhou, J. Meng, and P. Ring, *Phys. Rev. C* **68**, 034323 (2003).
- [60] K. Zhang, M. K. Cheoun, Y. B. Choi, P. S. Chong, J. Dong, L. Geng *et al.*, *Phys. Rev. C* **102**, 024314 (2020).
- [61] K. Takahashi, M. Yamada, and T. Kondon, *At. Data Nucl. Data Tables* **12**, 101 (1973).
- [62] T. Suzuki, *Phys. Lett. B* **104**, 92 (1981).
- [63] T. Suzuki and M. Yamada, *Nucl. Phys. A* **379**, 110 (1982).
- [64] S. Fracasso and G. Colò, *Phys. Rev. C* **76**, 044307 (2007).
- [65] P. W. Zhao, Z. P. Li, J. M. Yao, and J. Meng, *Phys. Rev. C* **82**, 054319 (2010).
- [66] A. R. Samana, C. Barbero, S. B. Duarte, A. J. Dimarco, and F. Krmpotić, *New J. Phys.* **10**, 033007 (2008).
- [67] M. R. de Azevedo, R. C. Ferreira, and C. A. Barbero, *Braz. J. Phys.* **50**, 466 (2020).
- [68] N. Paar, T. Nikšić, D. Vretenar, and P. Ring, *Phys. Rev. C* **69**, 054303 (2004).
- [69] K. Pham *et al.*, *Phys. Rev. C* **51**, 526 (1995).
- [70] H. Akimune *et al.*, *Phys. Rev. C* **52**, 604 (1995).
- [71] A. Krasznahorkay, H. Akimune, M. Fujiwara, M. N. Harakeh, J. Janecke, V. A. Rodin, M. H. Urin, and M. Yosoi, *Phys. Rev. C* **64**, 067302 (2001).
- [72] M. Wang, W. Huang, F. Kondev, G. Audi, and S. Naimi, *Chin. Phys. C* **45**, 030003 (2021).
- [73] G. Audi, F. G. Kondev, M. Wang, W. J. Huang, and S. Naimi, *Chin. Phys. C* **41**, 030001 (2017).
- [74] See Supplemental Material at <http://link.aps.org/supplemental/10.1103/PhysRevC.106.054318> for the data table of  $\beta$ -decay half-lives.